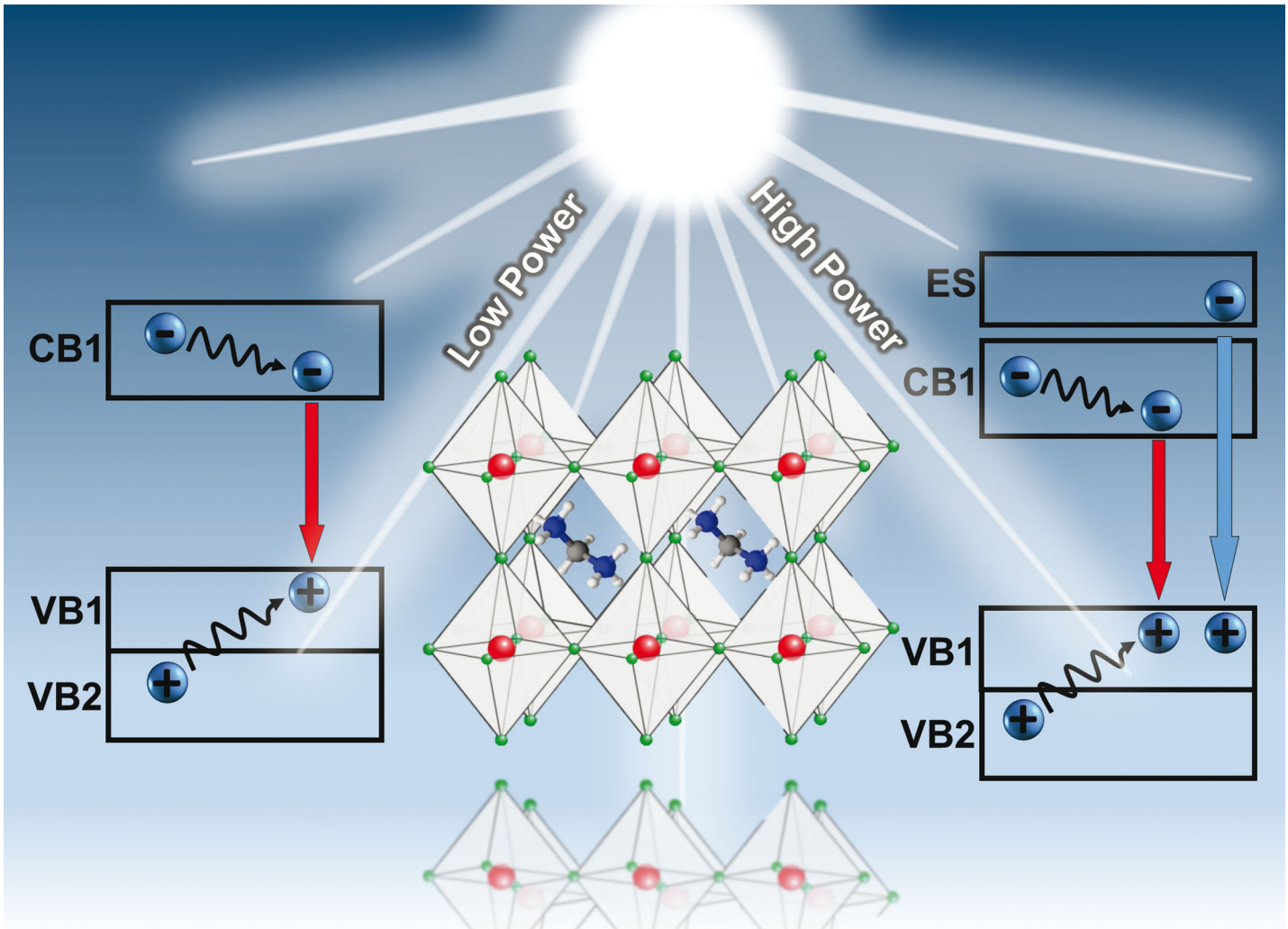

Showcasing work from the group of Prof. Abderrazzak Douhal, Universidad de Castilla-La Mancha, Toledo, Spain.

Title: How photon pump fluence changes the charge carrier relaxation mechanism in an organic–inorganic hybrid lead triiodide perovskite

Time-resolved UV-visible-NIR transient absorption and terahertz measurements reveal pump fluence-dependent mechanisms of charge carrier recombination in $FAPbI_3$ thin films. At low fluences of the absorbed photons, the conduction band (CB1) is depopulated to two valence bands (VB1 and VB2). The behavior of the perovskite film indicates charge carrier migration between VB2 and VB1. Increasing the pump fluence results in an additional excited state at energies higher than that of CB1, opening a new deactivation channel. The efficient Auger recombination in $FAPbI_3$ as compared to methylammonium lead triiodide suggests a higher density of states in the former.

As featured in:

See Abderrazzak Douhal *et al.*, *Phys. Chem. Chem. Phys.*, 2016, **18**, 27090.

ROYAL SOCIETY OF CHEMISTRY

www.rsc.org/pccp

Registered charity number: 207890

PCCP

PAPER

View Article Online
View Journal | View Issue

Cite this: *Phys. Chem. Chem. Phys.*, 2016, **18**, 27090

How photon pump fluence changes the charge carrier relaxation mechanism in an organic–inorganic hybrid lead triiodide perovskite†

Piotr Piatkowski,[a] Boiko Cohen,[a] Samrana Kazim,[b] Shahzada Ahmad[b] and Abderrazzak Douhal*[a]

This study explores the excitation wavelength and fluence dependence of processes occurring in formamidinium lead triiodide ($FAPbI_3$) film using time-resolved transient absorption and terahertz spectroscopies. The results indicate that second-order processes are responsible for charge carrier recombination at low fluences of the absorbed photons (below 8.4×10^{12} ph per cm^2). An increase in fluence leads to the appearance and successive reduction of the time component assigned to the Auger recombination of free charge carriers (240–120 ps). Simultaneously, the bimolecular recombination time decreases from ~1400 to ~700 ps. Further increasing the pump fluence produces an exciton population that recombines in 6 ps. The comparison of two characteristic bleaching bands located at 480 and 775 nm provides evidence for the validity of the two valence bands model. Excitation with higher fluences results in a marked difference in the probed dynamics at these bands, reflecting the action of two excited states at the conduction band. Our results demonstrate that a single model cannot be applied in characterizing the perovskite absorber transitions at all pump fluences. These findings are relevant in understanding their operating mechanism under specific experimental conditions, which should differ for perovskite based solar cells, lasing media or photon detectors.

Received 21st April 2016,
Accepted 6th June 2016

DOI: 10.1039/c6cp02682f

www.rsc.org/pccp

1. Introduction

Hybrid organic–inorganic trihalide perovskites have emerged as attractive absorbers for highly efficient photovoltaic devices.[1–7] The advantages of these materials are based on their high and broad absorption, which leads to the efficient generation of free charge carriers characterized by slow recombination and relatively high mobility.[8–10] Simultaneous improvements in absorber composition and solar cell architecture have resulted in power conversion efficiencies (PCE) higher than 22%.[1,4,11–15] The state of the art in this field is a recently reported formamidinium lead triiodide ($FAPbI_3$) sensitized device.[1] Despite the impressive performance of the $FAPbI_3$ based solar cell, there are only a handful of reports on the ultrafast fundamental processes in this material.[5,6,16,17] Time-resolved fluorescence spectroscopy has shown unbalanced electron and hole mobilities in $FAPbI_3$, leading to longer diffusion lengths in comparison with $MAPbI_3$.[2,6,7,16,18] In a recent report, the diffusion lengths of free charge carriers in $FAPbI_3$ and $FAPbBr_3$ single crystals were estimated to be 6.6 μm and 19 μm, respectively.[18] These high values were explained in terms of the low concentration of traps in the single crystals.[18] It was shown that the $FAPbBr_3$ crystal is characterized by a diffusion distance 5 times longer and dark carriers concentration 10 times lower than those of the $MAPbI_3$ crystal. Long diffusion lengths of 3.4 and 25 μm in two different $FAPbI_3$ thin polycrystalline films have also been reported.[5,16] The difference in the observed values was explained in terms of the different crystallinity and morphology of the studied samples.[16] Recent THz spectroscopic studies have demonstrated a relatively high charge carrier mobility of 27 $cm^2\ V^{-1}\ s^{-1}$ for a $FAPbI_3$ thin polycrystalline film.[5] A higher charge carrier mobility of 75 $cm^2\ V^{-1}\ s^{-1}$, which remains constant for at least 8 ns, has been reported for a $FAPbI_3$ thin film composed of large crystallites.[16] On the other

[a] *Departamento de Química Física, Facultad de Ciencias Ambientales y Bioquímica and INAMOL, Universidad de Castilla-La Mancha, Avenida Carlos III, Sin Número, 45071 Toledo, Spain. E-mail: abderrazzak.douhal@uclm.es; Tel: +34-925-265717*

[b] *Abengoa Research, Abengoa, Campus Palmas Altas, C/Energia Solar, 41014 Sevilla, Spain*

† Electronic supplementary information (ESI) available: Equation for the calculation of photon fluence. Description of the inverse of ΔOD dependence on the pump–probe delay time. Tables listing the values of the time constants and normalized (to 100) pre-exponential factors for the $FAPbI_3$ film upon excitation at 600 and 800 nm. Transient absorption vis-NIR spectra of the $FAPbI_3$ film upon excitation at 400 and 800 nm. Transient absorption spectra in the region between 470–560 nm. Transient absorption decays of the excited $FAPbI_3$ film. The inverse of ΔOD^{-2} with pump–probe delay time. The comparison of transient absorption and terahertz kinetics upon excitation at 400 and 800 nm. See DOI: 10.1039/c6cp02682f

hand, excitation of the same sample at 800 nm resulted in a reduction of the mobility to 40 $cm^2 V^{-1} s^{-1}$, suggesting the presence of shallow sub-bandgap states.[16] Furthermore, time-resolved THz studies have shown that the majority of the free charges (90%) are formed instantaneously after excitation, while the exciton population (10%) with higher binding energy dissociates in 20 ps.[16]

A deeper understanding of perovskites electronic structure, exciton dissociation, charge carrier separation, trapping and recombination is important in unravelling the operating mechanism boosting the efficiency of these solar cells and in improving their stability.[16,19–25] Furthermore, the potential of perovskites for application in lasers, light emitting diodes (LEDs) and photodetectors requires additional studies into their photobehavior at a high density of generated charges.[20,26–30] One of the open questions relates to the nature of the band transitions in these absorbers. Two models of band structure are usually invoked to explain the optical properties of the commonly used methylammonium lead triiodide perovskite ($MAPbI_3$).[7,19–21,31,32] The first one explains the recombination of the charge carriers with the presence of two valence bands (VBs) and one conduction band (CB).[7,31–33] Another model proposes a dual excited state composed of a charge transfer (CT) band and a charge separated band gap state.[19,20] Furthermore, theoretical study on the electronic structure of $MAPbI_3$ suggests that the existence of two conduction bands is responsible for transitions in this material.

Herein we present and discuss our studies on the ultrafast photoevents in a $FAPbI_3$ thin polycrystalline film, studied using time-resolved transient absorption (TA) and terahertz (THz) spectroscopies. In contrast to previous reports on the power dependent photobehavior of $MAPbI_3$,[8,21,25,31] we found that the contribution of Auger recombination to the processes of excited charge carrier deactivation in the $FAPbI_3$ film increases significantly with the fluence of the absorbed photons. Furthermore, the rise of the excited charge carrier density leads to the efficient formation of excitons that disappear in 6 ps. The differences between the behavior of the 480 and 775 nm decays, upon excitation at 400 nm with increasing fluence of the absorbed photons, indicate the existence of two excited states involved in the processes of charge carrier deactivation. The spectral and dynamical differences between the TA spectra in the 460–520 nm region upon excitation at 400 and 800 nm with different fluences of the absorbed photons suggest the presence of a transition between two valence bands.

2. Experimental part

2.1 Femtosecond transient absorption spectrometry

The femtosecond (fs) transient UV-visible absorption spectroscopy setup used here has been described elsewhere.[34] The fs-transient UV-visible-near IR experiments were performed using a chirped pulse amplification setup. It comprises a Ti:sapphire oscillator (TISSA 50, CDP Systems) pumped by a 5 W diode laser (Verdi 5, Coherent). The seed pulse (30 fs, 450 mW at 86 MHz) centred at 800 nm is directed to an amplifier (Legend-USP, Coherent). The amplified fundamental beam (50 fs, 1 Watt, 1 kHz) is directed through an optical parametric amplifier (OPA) for wavelength conversion (CDP Systems).[34] An 800 nm beam and its second harmonic (400 nm) or the second harmonic of the output of the OPA (600 nm) were used as the pump. The ratio of the spot size of the pump with respect to the probe was always bigger than 3 : 1. The spot size was measured using the razor (knife)-edge method.[35]

2.2 Sub-picosecond time-resolved terahertz spectrophotometry

The time-resolved THz setup is described elsewhere.[16] The amplified fundamental beam centered at 800 nm (50 fs, 1 W, 1 kHz) is split into three parts. The first one ($\sim$700 mW) is doubled in a 1 mm BBO crystal or it is first converted by an optical parametric amplifier and then doubled in a 1 mm BBO crystal to give the desired pumping wavelength. The resulting beam is sent through a long (up to 10 ns) delay line (H2W Technologies) to excite the sample in the time-resolved THz experiment. The second part of the fundamental beam ($\sim$200 mW) generates the THz probe in a ZnTe crystal by optical rectification. The third part ($\sim$1 mW) is used for the electro-optic detection of THz in another ZnTe crystal. During the measurements, the setup is continuously purged with dry nitrogen.

3. Results and discussion

3.1 Visible-NIR transient absorption spectroscopy

To begin with, we present and discuss the visible-NIR transient absorption spectroscopy (TAS) findings and decays of the black cubic structure of the $FAPbI_3$ thin polycrystalline film ($\sim$210 nm),[16] upon excitation at 400 and 800 nm, using four different fluences of the absorbed photons: 0.72, 1.2, 2.1 and 9.4 (10^{13} photons per cm^2 (ph per cm^2)). The synthesis procedure and X-ray structural characterization of the sample are given in detail in our previous report.[16]

Pumping at 400 nm, the transient absorption spectrum at 200 fs consists of two negative bands with intensity maxima located approximately at 500 nm (bleaching band, PB1) and 790 nm (bleaching band and stimulated emission, PB2), while the two regions between 530–740 nm and 850–1050 nm have positive signals (Fig. S1a, ESI†). The excitation of the $FAPbI_3$ film leads to a depopulation of the VB resulting in the ultrafast bleaching signals, which is similar to the findings of previous reports on the ultrafast dynamics of $MAPbI_3$.[7,31,32] The positive bands in the visible and NIR regions are formed as a result of the photoinduced absorption of hot electrons (in the CB) and holes (in the VBs). At 5 ps pump–probe delay time, the maximum intensity of the bleaching band at $\sim$505 nm shifts by 15 nm to a shorter wavelength, while the negative signal at $\sim$700 nm is converted to a positive one. The positive band in the NIR region, due to hot electrons and holes cooling within the conduction and valence bands, becomes negative as a result of the stimulated emission from the edge of the CB or trap

states recovering (Fig. S1a, ESI†).[22,31] Excitation at 800 nm leads to charge formation at the bottom of the VB (holes) and CB (electrons). As a result, the TA spectra at 0.2 and 5 ps are almost the same, reflecting the absence of electrons and holes cooling, in agreement with the reported behavior for the $MAPbI_3$ film (Fig. S1b, ESI†).[16,31] The TA spectra of $FAPbI_3$ do not differ from those of $MAPbI_3$, suggesting comparable spectral and temporal behaviors, thus supporting the spectral features assignment for $FAPbI_3$.[4,22,31]

It is commonly accepted that the PB2 for $FAPbI_3$ and $MAPbI_3$ is attributed to excitonic absorption leading to band filling.[5,21,28,36,37] Moreover, the presence of free charge carriers bleaches the excitonic transitions and thus additionally contributes to the TA spectra.[28,38] However, the origin of PB1 is still under debate.[7,19,37] Several explanations of the dynamical behavior in this region exist, which take into account additional excited and ground electronic states. The nature of these states will be discussed in detail below (*vide infra*).[7,19,39,40] To get a deeper insight into the photobehavior of PB1, we studied the excitation wavelength and fluence dependent characteristics of the TA spectra below <520 nm.

Upon excitation at 400 nm for pump–probe delay times below 500 fs, the bleaching signal located in the 470–520 nm region is composed of two overlapping bands centered approximately at 490 and 505 nm (Fig. 1a–c and Fig. S2, S3, ESI†). Their dynamics exhibit a 0.3 ps rising (480 nm) and decaying (505 nm) component, reflecting a hole transition between two ground electronic states (Fig. 2).[7,31,33] The increase in the absorbed photons density results in a reduction of the 505 nm band intensity in comparison with that at 490 nm (Fig. 1a–c). The decrease in the relative amplitude at 505 nm at higher fluences of the absorbed photons (2.1×10^{13} and 9.4×10^{13}) might be a result of the increasing contribution of the population with a maximum at 490 nm. Another possibility could be a decrease in the absorption cross-section of the band at 505 nm. The faster decay of the bleaching band with the increasing fluence of the absorbed photons is attributed to the rise of the excited charge carrier density leading to more efficient bimolecular deactivation and to Auger recombination, in agreement with previous reports on $FAPbI_3$ and $MAPbI_3$ films.[10,16,20,21,31]

The TA spectra of the $FAPbI_3$ film upon excitation at 800 nm with different fluences of the absorbed photons contain only

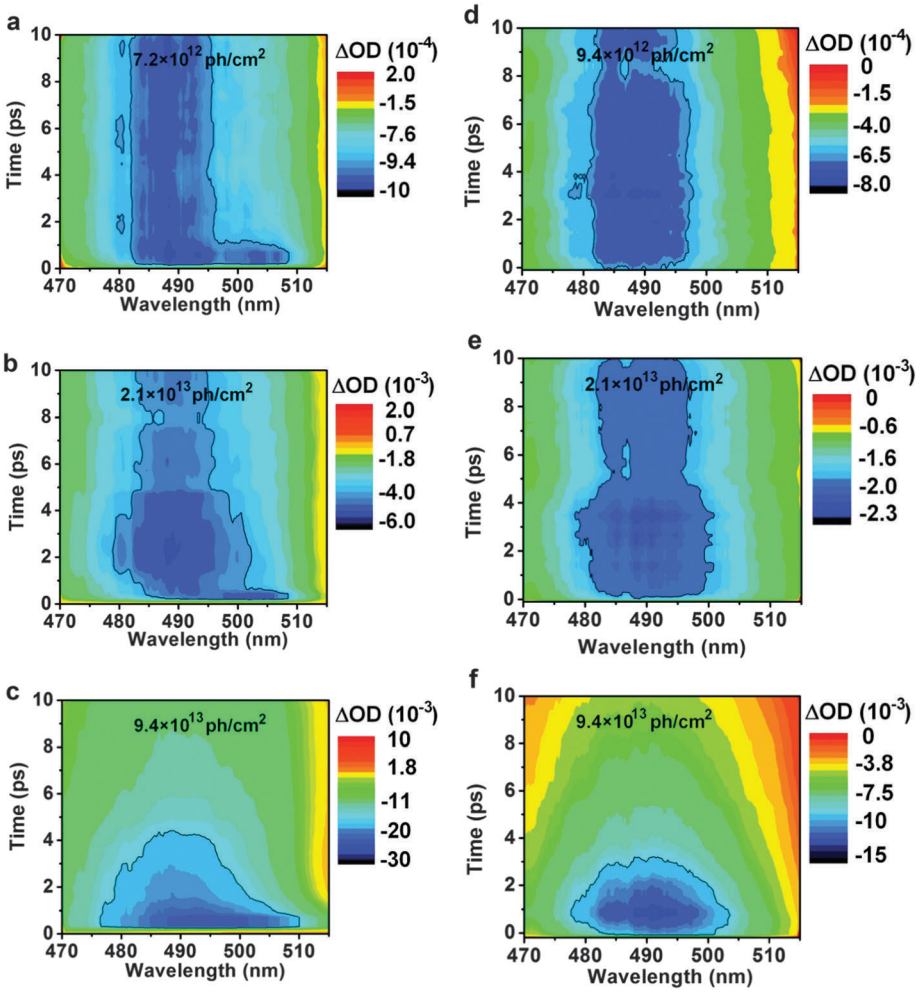

Fig. 1 Two dimensional pseudo-color ΔOD maps for the $FAPbI_3$ film upon excitation at (a–c) 400 nm and (d–f) 800 nm as a function of both wavelength and pump–probe delay time at different photon fluences (inset).

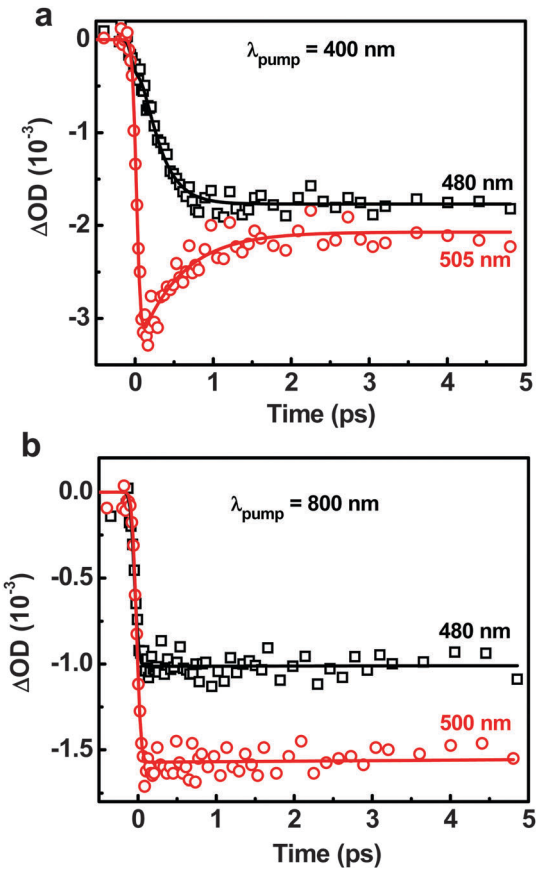

Fig. 2 Transient absorption kinetics of the $FAPbI_3$ film upon excitation at (a) 400 nm and (b) 800 nm using a fluence of absorbed photons of 1.2×10^{13} ph per cm^2. The probe wavelengths are indicated in the inset. The solid lines are from the best multi-exponential fits of the experimental data.

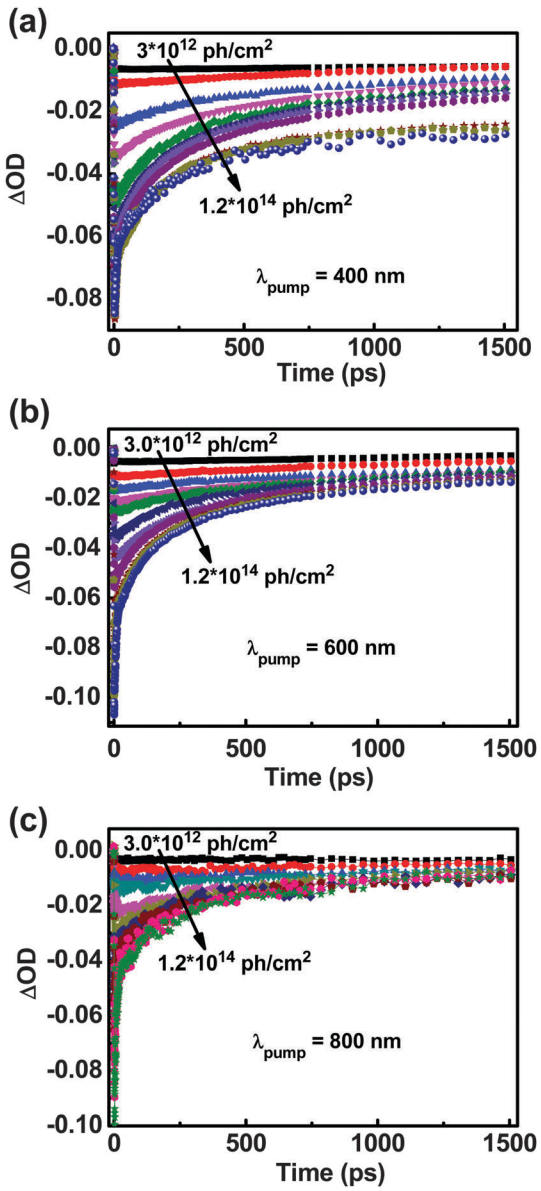

Fig. 3 Transient absorption decays of the $FAPbI_3$ film (λ_{obs} = 775 nm) upon excitation at (a) 400 nm, (b) 600 nm and (c) 800 nm at different photon fluences.

one band located at 490 nm (Fig. 1d–f). As the excitation at this wavelength (1.5 eV *vs.* 1.45 eV of the band gap) leads to charge carrier formation on the edges of the CB (electrons) and VB (holes), the holes with an excess energy over the top of the VB are not formed and the 505 nm spectral component is not present. The absence of a hole migration process results in the lack of the rising and decaying components at 490 and 505 nm for the $FAPbI_3$ film (Fig. 2b). Moreover, in agreement with the results for $FAPbI_3$ excitation at 400 nm, the increase in the pump fluence speeds up the second- and third-order recombination processes (bimolecular and Auger recombination).

3.2 Femtosecond dynamics at 775 nm observation wavelength

We first present and discuss the transient absorption decays at 775 nm observation wavelength, upon excitation at 400, 600 and 800 nm, with fluences of the absorbed photons between 3.0×10^{12} to 1.2×10^{14} (ph per cm^2), calculated using eqn (S1) (ESI†). The excitation wavelengths were chosen to generate electrons and holes with different excess energies as compared to the band gap of $FAPbI_3$ ($E_g \sim 1.45$ eV).[5,16,41,42] To analyze the dynamical behavior, we have chosen an observation wavelength (775 nm) located in the bleach band attributed to the VB depopulation of the excited perovskite (Fig. S1, ESI†).[16,19,20]

Fig. 3 shows the results upon excitation using various photon energies with different fluences of the absorbed photons. Fig. S4 (ESI†) shows the same transients, but in a short time window. The increase in the fluence clearly affects the TA kinetic traces, resulting in the appearance of new decaying components and in shortening of the existing ones. Table 1, as well as Tables S1 and S2 (ESI†), give the results using a multi-exponential fitting model. For all of the excitation wavelengths, we can distinguish three processes represented by groups of TA signals that depend on the variation of the fluence of the absorbed photons and are characterized by different dynamical behavior: (1) TA kinetics dominated by one process with time constants longer than that

Table 1 Values of the time constants (τ_i) and normalized (to 100%) amplitudes (A_i) of the multi-exponential functions used to fit the transient absorption signals of the excited $FAPbI_3$ film. The excitation was at 400 nm with different photon fluences, and the observation wavelength was 775 nm. The estimated errors in τ_i are: $\tau_1 \pm 10$ ps, $\tau_2 \pm 2$ ps, $\tau_3 \pm 40$ ps and $\tau_4 \pm 100$ ps. The transients were globally fitted using multi-exponential functions. A negative or positive sign before A_i indicates a decaying or a rising component

Fluence (10^{13} ph per cm^2)	A_1 (%)	τ_1 (ps)	(−) A_2 (%)	τ_2 (ps)	(−) A_3 (%)	τ_3 (ps)	(−) A_4 (%)	τ_4 (ps)	(−) Offset (%)
0.30	—	—	—	—	—	—	100	>1500	—
0.72	—	—	—	—	—	—	100	>1500	—
0.84	—	—	—	—	25	279	55	1390	20
1.1	—	—	—	—	30	187	53	1130	17
1.6	—	—	—	—	35	137	44	733	21
2.1	—	—	8	4	33	118	42	669	17
2.8	—	—	13	4	31	114	38	638	17
4.2	—	—	18	5	29	115	35	635	18
6.9	—	—	21	5	27	128	25	516	27
9.4	—	—	22	6	25	122	26	402	27
12	—	—	23	6	27	120	25	459	25

of the interrogated window (1.5 ns), (2) traces characterized by the contribution of two decaying components and (3) kinetics described by three components (Scheme 1a). Additionally, the first and the second group for excitation wavelengths of 600 and 800 nm show a rising component.

Except for the TA decays in the first group, those at higher fluences of the absorbed photons show offsets representing first-order (trap-assisted) recombination in the $FAPbI_3$ film. The lack of the offset at low fluences is due to the presence of a long positive decay component (beyond the time window of the TA experiment). Upon excitation at 600 and 800 nm, the offset is similar across the full range of fluences and its value amounts to 15–20%. This suggests that under these experimental conditions, the trap states are filled with charge carriers for the used fluences. The offset value for $FAPbI_3$ upon pumping at 400 nm is similar to those observed at longer excitation wavelengths when the fluence of the absorbed photons is in the range between 3.0×10^{12} and 4.2×10^{13} ph per cm^2, while at higher fluences we observed an increase to 25–27%. For $MAPbI_3$ it was shown that the high density of excited charge carriers with a large excess energy can result in the thermal activation of trap states.[23,43] Thus, the increase of the offset contribution can be assigned to the presence of trap states activated by the high number of absorbed photons with an energy exceeding that of the band gap.

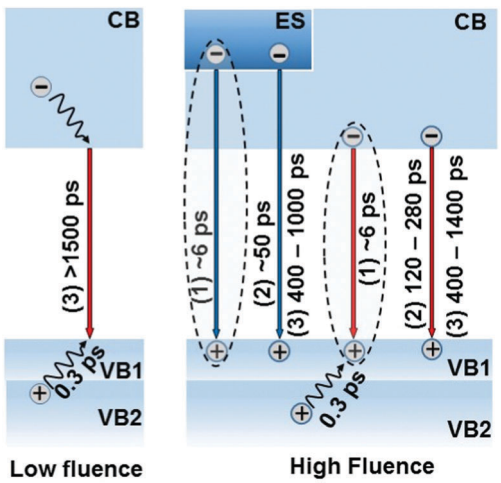

Scheme 1 Schematic representation of the recombination processes of (1) exciton and free charge carriers ((2) Auger and (3) second-order).

3.2.1. First group of TA decays. The TA decays in the first group (fluences between 0.3×10^{13} and 0.7×10^{13} ph per cm^2) arise from electron–hole (bimolecular) recombination (τ_4) of charge carriers in the $FAPbI_3$ film. The small exciton binding energy in lead iodide perovskites (5–50 meV) results in a fast and efficient electron–hole dissociation giving rise to free charge carriers characterized by relatively high mobility.[3–5,44] It was reported that the recombination processes in $MAPbI_3$ upon excitation with fluences similar to those used here lead to second-order deactivation of the excited charges.[8,16,20,25,44] Recently, bimolecular recombination was also suggested for $FAPbI_3$ thin film using terahertz spectroscopy.[16] Furthermore, as the transient absorption signal is proportional to the charge carriers concentration, the second-order nature of the observed phenomenon in $FAPbI_3$ is revealed by a linear dependence of the inverse of ΔOD on the pump–probe delay time at a fluence of 7.2×10^{12} ph per cm^2 (Fig. 4 and eqn (S2), ESI†). For the $MAPbI_3$ film, the linear trend of ΔOD^{-1} indicates that the dynamics upon excitation with a broad range of pump fluences are dominated by direct electron–hole recombination.[21,31,45–47] A deviation of ΔOD^{-1} from linearity has been reported only for relatively high pump fluences due to the weak contribution of Auger-type processes.[31]

3.2.2. Second group of TA decays. Increasing the fluence (second group), results in a higher density of initially generated charge carriers, and thus in a larger probability of both electron–hole recombination and many-body interactions (mostly Auger recombination of free charge carriers).[21,48,49] Upon excitation at 400 nm, the second group comprises fluences of between 8.4×10^{12} and 1.6×10^{13} ph per cm^2, while in the cases of 600 and 800 nm excitation, this group also includes fluences of up to 2.8×10^{13} and 2.1×10^{13} ph per cm^2, respectively (Fig. 3, 4a, Table 1 and Tables S1, S2, ESI†). The result of Auger recombination (three-body process) is the appearance of a new decay component (τ_3) and the decrease of the τ_4 value. Furthermore, as the dynamics of three-body interactions are characterized by

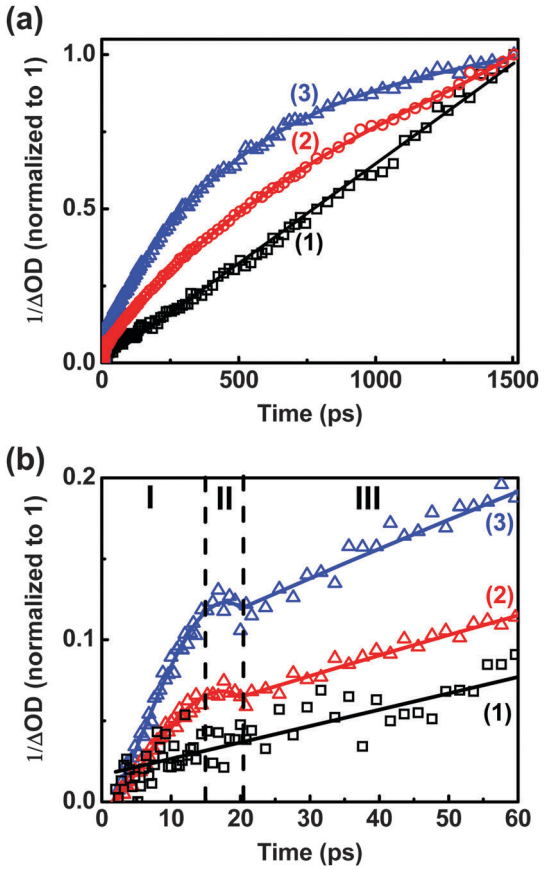

Fig. 4 (a) Variation of the inverse of ΔOD with pump–probe delay time for the $FAPbI_3$ film upon excitation at 400 nm and observation at 775 nm. (b) The same as in (a) but in a shorter time window. The fluences of the absorbed photons (ph per cm^2) were (1) 7.2×10^{12} (black squares), (2) 4.2×10^{13} (red triangles) and (3) 6.9×10^{13} (blue circles). The solid lines are to guide the eye.

the linear dependence of the inverse square of ΔOD on the pump–probe time delay (eqn (S3), ESI†),[50] we observe the deviation of ΔOD^{-1} from linearity (Fig. 4a). Similar behavior has been observed for $MAPbI_3$ films.[8,21,51] Fig. S5 (ESI†) shows that the ΔOD^{-2} upon excitation at 400 nm using an absorbed pump fluence of 6.9×10^{13} ph per cm^2 is linear between 40–900 ps. The deviation from linearity for pump–probe delay times longer than 900 ps is due to the second-order processes of free charge deactivation (Fig. S5, ESI†). The presence of Auger recombination characterized by three different times (9, 75 and 450 ps) was previously reported in a $MAPbI_3$ thin film.[51] Furthermore, it was shown that the time constant for bimolecular recombination decreases by more than an order of magnitude when the density of the excited charge carriers increases.[21]

In contrast to $MAPbI_3$, where the dynamics were dominated by bimolecular deactivation even at relatively high pump fluences, those in $FAPbI_3$ are strongly affected by Auger recombination (Fig. 3, 4, Table 1 and Tables S1, S2, ESI†).[21,31,45] It was reported that changing methylammonium to formamidinium results in a change in the perovskite band structure, giving rise to unbalanced electron and hole mobilities.[6] In agreement with this statement, the efficient third-order recombination in $FAPbI_3$ also proves the differences in the electronic structure of both materials.[6] The process of third-order recombination in semiconductors is strongly affected by the energy and momentum conservation requirements that limit the density of final states, and thus it strongly depends on the band structure.[43] Although the contribution of Auger recombination is not important in the solar cell under AM1.5 illumination, it becomes significant for lasing applications due to the high charge densities induced in the active medium.

For the first and second group of the TA decays, pumping at 600 and 800 nm, an additional rising component (τ_1 = 10–30 ps) with a small amplitude (6–14%) has been observed (Fig. S6a and Tables S1, S2, ESI†). This component is attributed to the rise of the free charge carrier population due to exciton dissociation within the first 20 ps, and is similar to that observed in a previous report.[16] The major part of the free charge carriers (90%) in $FAPbI_3$ is formed instantaneously (within the IRF), while 10% of excitons with a higher binding energy dissociate in 20 ps.[16] The contribution of this component decreases, and disappears in the third group of transients, upon increasing the fluence of the absorbed photons, due to the increasing contribution of the ultrafast component (Tables S1 and S2, ESI†).

3.2.3. Third group of TA decays. The third group of transients is characterized by the appearance of an additional ultrafast decaying component (τ_2), which we assign to fast exciton or Auger exciton–exciton recombination (Fig. 3, Table 1 and Fig. S4, Tables S1, S2, ESI†).[48,49] The presence of this component results in a rise of the inverse of ΔOD (in less than 20 ps) followed by a slower one assigned to free charge carrier deactivation (Fig. 4b). This new behavior suggests that two different populations (excitons and free charges) are responsible for the dynamics of the system at short and long delay times.[32,45,52] It has been reported that at high pump fluences the equilibrium between free charge carriers and excitons present in the $MAPbI_3$ film is shifted in favor of exciton formation.[4,36] Recently, the results of femtosecond transient absorption microscopy evidenced the coexistence of excitons and free charges in $MAPbI_3$.[53] However, the contribution of the exciton population to the TA dynamics observed in the visible part of the spectrum for $MAPbI_3$ films under ambient conditions has not been observed. The higher probability of electron–hole bound pair formation results from the high density of initially generated species that interfere with the processes of charge carrier creation and migration. An ultrafast component (~3 ps) that indicates the excitonic nature of the transition in $MAPbI_3$ at 77 K was observed at high pump energies.[45] Furthermore, the time-resolved TA measurements of $MAPbI_3$ under ambient conditions in the NIR region (1500 nm band) have shown the presence of excitons decaying in ~1 ps.[52]

To get further information about the existence of additional species present at high densities of excited charge carriers, we have carried out time-resolved THz measurements of the $FAPbI_3$ film when pumping at 400 and 800 nm. The increase in fluence of the absorbed photons leads to a shortening of the THz decays in the $FAPbI_3$ film (Fig. S7–S10, ESI†). In the current study, we observed faster decays of the THz signals than those presented in a previous report.[16] The difference in the observed

behavior is explained in terms of the more efficient higher-order processes of recombination at larger charge carrier densities.[16] Fig. S7–S10 (ESI†) show that the TA and THz decays at a fluence of the absorbed photons of 0.72×10^{13} ph per cm^2 are the same, which demonstrates that the observed mobility is due to a drop in the excited free charge carrier concentration.[16,44] In contrast to the TA decays upon excitation at a fluence of 9.4×10^{13} ph per cm^2, the THz ones do not show the presence of the 6 ps component attributed previously to the decay of the excitons population. The lack of this component is due to the higher mobility of the free charge carriers in comparison with that of the excitons, and thus the signal resulting from electron–hole pairs is not visible. Furthermore, our previous report on the charge carrier mobility in a $FAPbI_3$ film showed that the THz spectra at 1 and 20 ps pump–probe time delays are similar, which additionally supports the assignment of the observed behavior to free charge carriers.[16] Thus the time-resolved TA data, along with the previous reports on $MAPbI_3$, present evidence for the exciton population at high fluences of the absorbed photons.[36,45,52]

Next, we compare and discuss the time constants attributed to the second- and third-order processes of the free charge carriers deactivation (τ_3 and τ_4), which show a dependence on the fluence of the absorbed photons across the 3 TA decay groups (Table 1 and Tables S1, S2, ESI†). The increase in the excited charge density with the fluence results in the shortening of τ_3 and τ_4, from $\sim$260 to $\sim$120 ps and from >1500 to $\sim$460 ps, independently of the excitation wavelength (400, 600 and 800 nm), taking into account the experimental error for τ_3 and τ_4 (40 and 100 ps, respectively). Furthermore, the amplitude of the τ_3 component increases relative to that of the τ_4 one when the pump fluence increases, indicating the more efficient contribution of Auger recombination (Table 1 and Tables S1 and S2, ESI†).[5,8] However, the component attributed to exciton recombination ($\tau_2 \sim 6$ ps) is independent of the density of excited charges formed at different excitation wavelengths with the used fluences. This suggests that the contribution of the Auger processes to exciton recombination is weak (Table 1 and Tables S1, S2, ESI†).

The linearity of the inverse of ΔOD as a function of the pump–probe delay time for different fluences indicates also that the excitons disappear predominantly due to the second-order process (region I in Fig. 4b and Fig. S11, ESI†). The dependence of the area (region II) located between region I, attributed to the recombination of excitons, upon that assigned to free charge carriers (region III) indicates a nonlinear behavior at intermediate fluences of 4.2×10^{13} and 6.9×10^{13} ph per cm^2 (Fig. 4b and Fig. S11, ESI†). Fig. S11 (ESI†) shows that the inverse of ΔOD as a function of the pump–probe delay time for $FAPbI_3$ upon excitation at 600 nm is also nonlinear in region II (Fig. 4b and Fig. S11, ESI†). This behavior suggests that part of the recombining excitons with excess energy can also dissociate, giving rise to a further increase in the free charges concentration. The excitation at 800 nm results in a smooth transition from region I to III (Fig. S11, ESI†). In the absence of excess energy, the photogenerated excitons do not dissociate efficiently, in agreement with a recent report showing that thermally activated exciton dissociation and recombination control the carrier dynamics in $MAPbI_3$.[31,54]

The relative amplitude (A_2) of the τ_2 component increases upon excitation with a decrease in photon energy, and also with its fluence (Fig. 3, Table 1 and Fig. S6b, Tables S1, S2, ESI†). This behavior suggests that the excess energy over the $FAPbI_3$ band gap results in more efficient exciton dissociation into free charges and/or the higher contribution of the excitonic states. The presence of excitons localized in sub-bandgap states has recently been reported for $MAPbI_3$ and $MAPbBr_3$ films.[22,55] A recent report on a $FAPbI_3$ film has shown the reduction of the charge carrier mobility from 75 to 40 $cm^2\ V^{-1}\ s^{-1}$ with the excitation wavelength changing from 500 to 800 nm, which also suggests the existence of energy states characterized by low charge carrier mobility at the bottom of the CB.[16] Excitation close to the edge of the CB may result in higher occupation of the sub-bandgap states, and thus in the rise of the τ_2 relative amplitude with a decrease in photon energy, as compared to those of the Auger and bimolecular recombination of the free charge carriers. It was shown that the absorption of photons with energy close to the band gap in a $FAPbI_3$ thin polycrystalline film results in more uniform initial charge carrier generation due to the higher penetration depth at longer wavelengths.[16] As the trapping events in perovskites are attributed mostly to the surface sub-bandgap states, this uniform distribution results in the higher relative contributions of excitons. Additionally, all time components at various excitation wavelengths are similar (Table 1 and Tables S1, S2, ESI†), which indicates that the observed changes are mainly due to differences in the relative contributions of the processes occurring in the $FAPbI_3$ film. Moreover, as the excitons formed at 800 nm do not have excess energy, they cannot dissociate efficiently into free charges, as discussed for the variation of ΔOD^{-1} with pump–probe delay times. The increase of A_2 with fluence of the absorbed photons is due to the higher initial density of excited charge carriers, which results in higher excitons contribution in the earliest stages of the time evolution of excited $FAPbI_3$.[23,36,43]

3.3 Comparison of the femtosecond dynamics at 480 and 775 nm observation wavelengths

Next, we studied the origin of the 460–520 nm bleaching band. We analyzed the TA decays at an observation wavelength of 480 nm by comparison with those probed at 775 nm, upon excitation at 400 nm and 800 nm with three different fluences of the absorbed photons ($0.72–9.4 \times 10^{13}$ ph per cm^2).

Upon excitation at 400 nm with the lowest fluence (7.2×10^{12} ph per cm^2), the transients at both interrogated wavelengths are identical (Fig. 5a and b), indicating that the bleaching bands are repopulated from a single excited state (CB), in agreement with previous reports.[7,31] Both sets of kinetics are dominated by the presence of a single process with a time constant longer than that of the used window (1.5 ns). The charge carrier recombination at this fluence can be attributed to a second-order (bimolecular) process in the $FAPbI_3$ film.[16,20,21] Further increasing the fluence (1.1×10^{13} ph per cm^2) gives rise to the appearance of two different decaying components for the

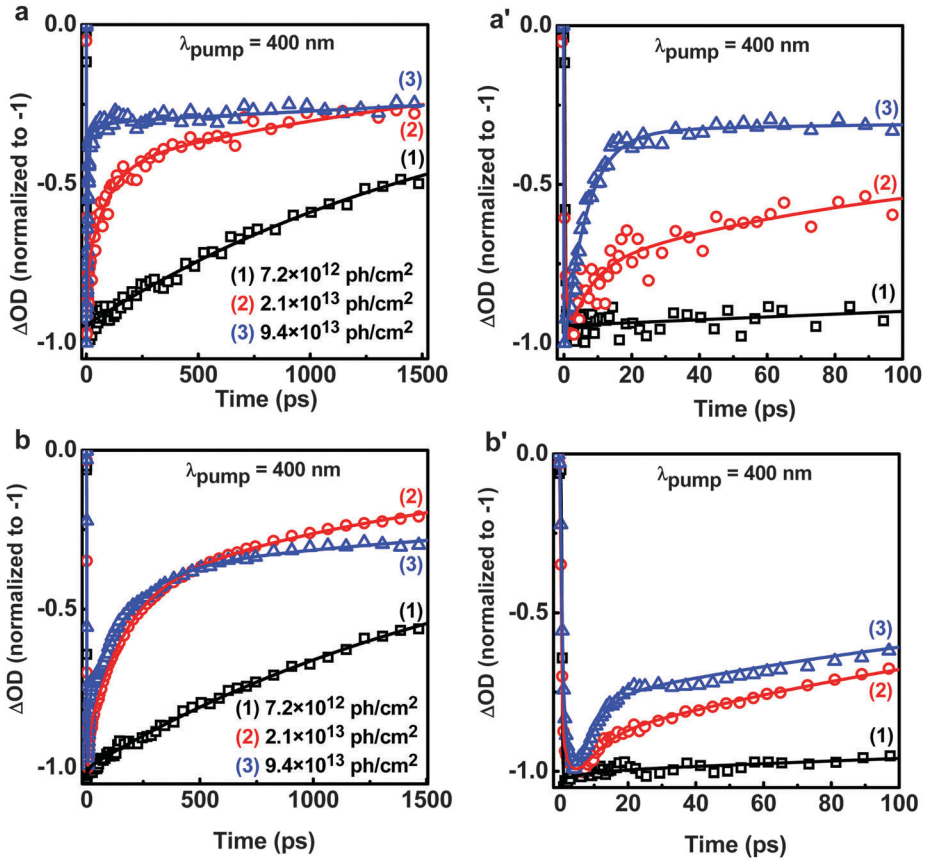

Fig. 5 TA decays for $FAPbI_3$ at (a and a′) 480 nm and (b and b′) 775 nm, upon excitation at 400 nm with the indicated photon fluences. Solid lines are from the best multi-exponential fits of the experimental data.

transients at 480 and 775 nm with time constants of τ_3 = 45 ps and τ_4 = 1060 ps at 480 nm and τ_3 = 187 ps and τ_4 = 1130 ps at 775 nm (Fig. S12, ESI†). At a fluence of 2.1 × 10^{13} ph per cm^2, three decaying components are present at the 480 and 775 nm observation wavelengths, τ_2 = 6 ps, τ_3 = 50 ps and τ_4 = 480 ps at 480 nm and τ_2 = 6 ps, τ_3 = 120 ps and τ_4 = 670 ps at 775 nm (Fig. 5). Finally, the highest fluence (9.4 × 10^{13} ph per cm^2) results in larger differences between the observed dynamics of the two bleaching bands (Fig. 5). The transient at 480 nm is bi-exponential, with an ultrafast 6 ps decay followed by a component longer than 1.5 ns, while the one at 775 nm indicates the presence of three components having values of τ_2 = 6 ps, τ_3 = 128 ps and τ_4 = 402 ps. The rise of the initial density of generated electrons and holes results in a larger probability of both the electron–hole (τ_4) and Auger (τ_3) recombination of free charges.[16,31]

The difference between the 480 nm and 775 nm transients of $FAPbI_3$ (Fig. 5), upon excitation at 400 nm with fluences of the absorbed photons of 2.1 and 9.4 (10^{13} ph per cm^2), suggests the involvement of two excited states in the process of electron deactivation at high fluences, in agreement with a previously suggested model.[19] Furthermore, the absence of the time components attributed to free charge carriers at 480 nm indicates that at high fluences, the PB1 results only from the excitons population. Additionally, the lack of the free charge carriers signature in the 480 nm transients suggests that the large density of the initially generated charges changes the local electronic structure of $FAPbI_3$, and thus the TA cross section of the excitons and free charges that absorb in the 470–520 nm region. Previously, we have experimentally shown that increasing the pump fluence results in the reduction of the absorption coefficient of a $MAPbI_3$ film.[31] Additionally, the TA spectra at 1.5 ns pump–probe delay time show that the bleaching band is broader at a higher fluence, and its structure contains the 505 nm signal (Fig. S2b, ESI†), explaining the differences between the optical properties of the film at different initial concentrations of excited charge carriers. On the other hand, as there are no differences between 480 and 775 nm transients at low excitation fluence (2.1 × 10^{13} ph per cm^2), we conclude that the contribution of an additional excited state or of structural changes are insignificant at a low density of initially excited charges, while at high fluences we observed spectral and dynamical evidence for the formation of a new excited state.

The TA kinetics at the 775 nm observation wavelength, interrogated in a 5 ps window, show the presence of an ultrafast rising component that becomes longer with an increase in the fluence of the absorbed photons (Fig. S13, ESI†). This behavior is attributed to a shift in the transition energies towards higher values upon pumping with higher fluences or to a photon bottleneck and states reorganization.[21,56] The rising components in the 480 nm signal have the same value at fluences of 0.72 and 2.1 × 10^{13} ph per cm^2.

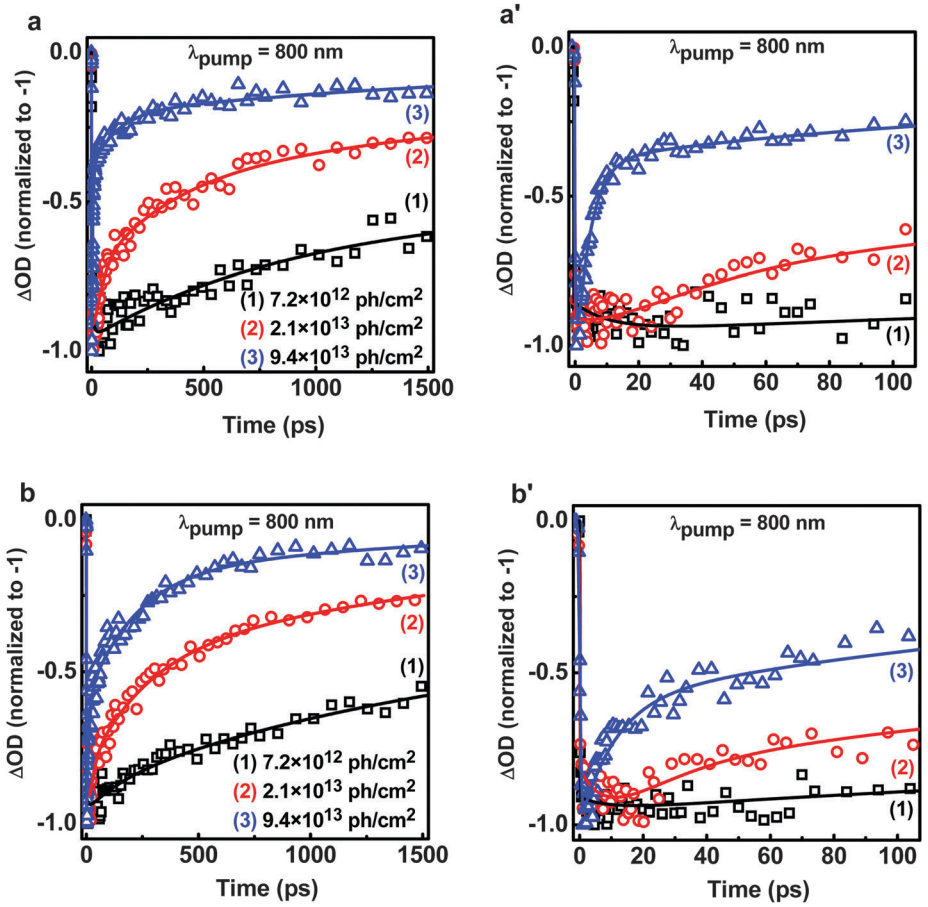

Fig. 6 TA decays for $FAPbI_3$ at (a and a′) 480 nm and (b and b′) 775 nm, upon excitation at 800 nm with the indicated photon fluences. Solid lines are from the best multi-exponential fits of the experimental data.

This component was previously assigned to the process of hole migration within VB states (*vide supra*). The TA kinetics at the 480 nm observation wavelength upon pumping using the highest fluence (9.4×10^{13} ph per cm^2) do not show the presence of this rising component due to the insignificant contribution of hole migration to the processes of VB recovery (Fig. S13b, ESI†). Furthermore, the lack of a fluence dependent increase in the value of the rising component at the 480 nm observation wavelength indicates that its origin differs from that observed at 775 nm.

Fig. 6 shows the normalized 480 and 775 nm transients upon excitation at 800 nm with different fluences of the absorbed photons. Pumping with 800 nm puts the system in a level at the CB with insignificant excess energy. However, increasing the fluence leads to a shortening of the time constant attributed to bimolecular recombination (τ_4), from a time that is longer than the interrogated time window (1.5 ns) to ~430 ps. Furthermore, the time components (6 ps and 100–120 ps) attributed to exciton and Auger recombination also appear. The increase in the pump fluence generates a higher initial density of excited charges, and thus opens the route to more efficient free charge carrier recombination and exciton formation.[23,36,43] Note that the 480 and 775 nm transients are very similar when using fluences of 0.72 and 2.1×10^{13} ph per cm^2 (Fig. 6). At 9.4×10^{13} ph per cm^2, the time components have the same values (Table S2, ESI†), but their amplitudes are different: A_2 = 78%, A_3 = 11%, A_4 = 11% at 480 nm and A_2 = 43%, A_3 = 19%, A_4 = 26% at 775 nm. In agreement with the photobehavior upon pumping at 400 nm, the 800 nm excitation at high photon densities (9.4×10^{13} ph per cm^2) leads to a change in the local structure in the $FAPbI_3$ film, and thus in the TA cross section of the excitons and free charges. The similarity of the decaying components at 800 nm excitation at the same fluences suggests the contribution of only one excited state to the processes of charge carriers deactivation. The additional energy level taking part in the electron–hole recombination upon excitation at 400 nm has an energy higher than that of the CB edge. This finding is additionally supported by the lack of the 505 nm band upon 800 nm excitation (Fig. 1d–f and Fig. S2, S3, ESI†). The transients at the 480 and 775 nm observation wavelengths upon excitation with different fluences of the absorbed photons pumping at 800 nm are characterized by an instantaneous rise, in contrast with those at the 400 nm excitation wavelength (Fig. S14, ESI†). This indicates the lack of hole transition between two different ground electronic states.

3.4 The origin of the ultrafast processes in $FAPbI_3$

Several models have been proposed to explain the ultrafast optical properties of $MAPbI_3$.[7,19] The first one was developed on

the basis of the similarity of the TA decays upon excitation at 400 and 600 nm at several observation wavelengths and the presence of ultrafast rising and decaying components (0.4 ps) at the negative signals, respectively. This model suggested the presence of two VBs and one conduction band.[7] The second model explained the ultrafast events in $MAPbI_3$ by proposing the existence of a dual excited state composed of a charge transfer (CT) state and charge separated band gap state.[19,20] In this model, the process of the CT state formation upon excitation at 387 nm (3.2 eV) is a result of photoinduced electron transfer from the iodide anion to the lead cation.[19] One of the arguments in support of this model was the observed difference between the time components gating at 480 nm (~100 ps) and 760 nm (310 ps), indicating the different origins of the charge relaxation to the ground state.[19] It is worth noting that these two models were based on observations using different experimental conditions, including the fluences produced by the laser pump. The two valence band model for $MAPbI_3$ films is based on results obtained at a low pump fluence of $\sim 2.2 \times 10^{12}$ ph per cm^2, while using a higher pump fluence ($\sim 3.7 \times 10^{13}$ ph per cm^2) suggests the presence of two excited states (CB and CT) in $MAPbI_3$.[7,19] A theoretical study on the electronic structure of $MAPbI_3$ proposed that the absorption features at 480 nm correspond to a direct transition between VB1 and CB1, with additional contributions from VB1–CB1 and VB1–CB2 transitions.[39] Recently, the ultrafast behavior observed in $MAPbI_3$ was attributed both to the phonon bottleneck process and to a band reorganization occurring directly after excitation with high photon density.[40]

In light of the presented data, we suggest that the photoinduced dynamics in the $FAPbI_3$ film reveal a model that involves two valence bands (VB1 and VB2) and two excited states (Scheme 1). Moreover, the contribution of the excited states becomes detectable in the PB1 region upon pumping at 400 nm with increasing fluence of the absorbed photons. The 0.3 ps rising (480 nm) and decaying (505 nm) component for the $FABbI_3$ sample upon excitation at 400 nm with all fluences of the absorbed photons (Fig. 2 and Fig. S15, ESI†), reflects hole migration between two valence bands (from VB2 to VB1) rather than the dynamical changes attributed to both the band renormalization and phonon bottleneck processes, which are sensitive to the fluence of the absorbed photons. It was evidenced for $MAPbI_3$ that a tenfold increase in the excited charge carrier density results in the retardation of the charge carriers cooling time from 230 to 770 fs.[40] In the case of the currently measured $FAPbI_3$, the increase in the fluence of the absorbed photons from 0.72 to 9.4×10^{13} ph per cm^2 has no effect on the decaying component at 505 nm (Fig. S15, ESI†). At the same time, the value of the 480 nm rising component remains the same for the two lower fluences and the component finally disappears upon excitation at a fluence of 9.4×10^{13} ph per cm^2 (Fig. S15, ESI†). The contribution of the two excited states to the photoinduced processes is supported by differences between the time components at the 480 and 775 nm observation wavelengths that become evident with the increase in the fluences of the absorbed photons upon excitation at 400 nm (Scheme 1). The lack of a dynamical signature of transitions between two CB states may suggest that the observed differences are not due to two conduction bands. Moreover, the power dependent differences between the dynamics at 480 and 775 nm indicate that the increase in the charge carrier density may lead to reversible local changes in the structure of $FAPbI_3$, which in turn give rise to new transitions in the host. The similar dynamical behavior of the kinetics at the 480 and 775 nm observation wavelengths upon 800 nm excitation with different fluences of the absorbed photons suggests that the transition represented by PB1 occurs from an electronic state located higher than the edge of the CB.

4. Conclusions

In conclusion, using fs TA and THz spectroscopy, we have characterized the generation and temporal evolution of excitons and free charge carriers in $FAPbI_3$ thin polycrystalline film, deposited on a glass. We found that the photoinduced events at low fluences of the absorbed photons ($3.0–7.2 \times 10^{12}$ ph per cm^2) are dominated by the second-order recombination of free charge carriers occurring on a timescale longer than 1.5 ns. The increase in the fluence results in the appearance and the subsequent shortening of the Auger recombination time (240–120 ps) assigned to free charges. Concomitantly, we see a reduction of the electron–hole recombination time (τ_4) from ~1400 to ~700 ps. Further increasing the fluence gives rise to an ultrafast decaying component, assigned to the process of exciton recombination ($\tau_2 \sim 6$ ps). The increase of the τ_2 component contribution with an increase in the energy of the excitation wavelength indicates that excitons with excess energy dissociate more efficiently into free charges. The time evolution of the TA spectra upon excitation at 400 and 800 nm along with the dynamical behavior of the two bleaching bands at 480 nm (PB1) and 775 nm (PB2), indicates the existence of two valence bands (VB2 and VB1) at low pump fluences (Scheme 1). Furthermore, the similarity of the TA transients at low fluence of the absorbed photons shows that PB1 and PB2 arise from the same ground state recovery (VB1). The differences between the time constants of the 480 nm and 775 nm transients upon excitation at 400 nm at high pump fluence suggest the existence of two excited states (Scheme 1). On the other hand, the similarities between the 480 and 775 nm transients upon excitation at 800 nm and at the used fluences put the additional excited state at an energy level higher than that of the CB edge. Our results clearly identify the action of two excited and two ground states in defining the photobehavior of the $FAPbI_3$ film, and give the experimental conditions and clues to the origin of the charge carriers recombination to the ground state. We believe that our findings provide new insights into the ultrafast processes occurring in $FAPbI_3$, covering a large spectral range and fluences of the exciting photons, and will help in improving the optimization of perovskite based solar cells.

Acknowledgements

This work was supported by MINECO and JCCM (Spain) through projects MAT2014-57646-P and PEII-2014-003-P. The work at Abengoa Research was supported by Quantcells project from CDTI and Torres Quevedo.

References

1 W. S. Yang, J. H. Noh, N. J. Jeon, Y. C. Kim, S. Ryu, J. Seo and S. I. Seok, *Science*, 2015, **348**, 1234–1237.
2 S. D. Stranks, G. E. Eperon, G. Grancini, C. Menelaou, M. J. P. Alcocer, T. Leijtens, L. M. Herz, A. Petrozza and H. J. Snaith, *Science*, 2013, **342**, 341–344.
3 R. Ohmann, L. K. Ono, H.-S. Kim, H. Lin, M. V. Lee, Y. Li, N.-G. Park and Y. Qi, *J. Am. Chem. Soc.*, 2015, **137**, 16049–16054.
4 H.-S. Kim, C.-R. Lee, J.-H. Im, K.-B. Lee, T. Moehl, A. Marchioro, S.-J. Moon, R. Humphry-Baker, J.-H. Yum, J. E. Moser, M. Graetzel and N.-G. Park, *Sci. Rep.*, 2012, **2**, 591.
5 W. Rehman, R. L. Milot, G. E. Eperon, C. Wehrenfennig, J. L. Boland, H. J. Snaith, M. B. Johnston and L. M. Herz, *Adv. Mater.*, 2015, **27**, 7938–7944.
6 G. E. Eperon, S. D. Stranks, C. Menelaou, M. B. Johnston, L. M. Herz and H. J. Snaith, *Energy Environ. Sci.*, 2014, **7**, 982–988.
7 G. Xing, N. Mathews, S. Sun, S. S. Lim, Y. M. Lam, M. Graetzel, S. Mhaisalkar and T. C. Sum, *Science*, 2013, **342**, 344–347.
8 C. Wehrenfennig, G. E. Eperon, M. B. Johnston, H. J. Snaith and L. M. Herz, *Adv. Mater.*, 2014, **26**, 1584–1589.
9 M. De Bastiani, V. D'Innocenzo, S. D. Stranks, H. J. Snaith and A. Petrozza, *APL Mater.*, 2014, **2**, 081509.
10 Z. Guo, J. S. Manser, Y. Wan, P. V. Kamat and L. Huang, *Nat. Commun.*, 2015, **6**, 7471.
11 J. H. Heo, S. H. Im, J. H. Noh, T. N. Mandal, C.-S. Lim, J. A. Chang, Y. H. Lee, H.-J. Kim, A. Sarkar, M. K. Nazeeruddin, M. Graetzel and S. I. Seok, *Nat. Photonics*, 2013, **7**, 487–492.
12 J.-W. Lee, D.-J. Seol, A.-N. Cho and N.-G. Park, *Adv. Mater.*, 2014, **26**, 4991–4998.
13 J. Burschka, N. Pellet, S.-J. Moon, R. Humphry-Baker, P. Gao, M. K. Nazeeruddin and M. Graetzel, *Nature*, 2013, **499**, 316–319.
14 M. Saliba, T. Matsui, J.-Y. Seo, K. Domanski, J.-P. Correa-Baena, M. K. Nazeeruddin, S. M. Zakeeruddin, W. Tress, A. Abate, A. Hagfeldtd and M. Gratzel, *Energy Environ. Sci.*, 2016, **9**, 1989–1997.
15 NREL chart, http://www.nrel.gov/ncpv/images/efficiency_chart.jpg, accessed 13.03.2016, 2016.
16 P. Piatkowski, B. Cohen, C. S. Ponseca, Jr., M. Salado, S. Kazim, S. Ahmad, V. Sundstrom and A. Douhal, *J. Phys. Chem. Lett.*, 2016, **7**, 204–210.
17 N. Pellet, P. Gao, G. Gregori, T.-Y. Yang, M. K. Nazeeruddin, J. Maier and M. Graetzel, *Angew. Chem., Int. Ed.*, 2014, **53**, 3151–3157.
18 A. A. Zhumekenov, M. I. Saidaminov, M. A. Haque, E. Alarousu, S. P. Sarmah, B. Murali, I. Dursun, X.-H. Miao, A. L. Abdelhady, T. Wu, O. F. Mohammed and O. M. Bakr, *ACS Energy Lett.*, 2016, **1**, 32–37.
19 K. G. Stamplecoskie, J. S. Manser and P. V. Kamat, *Energy Environ. Sci.*, 2015, **8**, 208–215.
20 J. A. Christians, J. S. Manser and P. V. Kamat, *J. Phys. Chem. Lett.*, 2015, **6**, 2086–2095.
21 J. S. Manser and P. V. Kamat, *Nat. Photonics*, 2014, **8**, 737–743.
22 X. Wu, M. T. Trinh, D. Niesner, H. Zhu, Z. Norman, J. S. Owen, O. Yaffe, B. J. Kudisch and X. Y. Zhu, *J. Am. Chem. Soc.*, 2015, **137**, 2089–2096.
23 S. D. Stranks, V. M. Burlakov, T. Leijtens, J. M. Ball, A. Goriely and H. J. Snaith, *Phys. Rev. Appl.*, 2014, **2**, 034007.
24 D. Shi, V. Adinolfi, R. Comin, M. Yuan, E. Alarousu, A. Buin, Y. Chen, S. Hoogland, A. Rothenberger, K. Katsiev, Y. Losovyj, X. Zhang, P. A. Dowben, O. F. Mohammed, E. H. Sargent and O. M. Bakr, *Science*, 2015, **347**, 519–522.
25 C. S. Ponseca, Jr., E. M. Hutter, P. Piatkowski, B. Cohen, T. Pascher, A. Douhal, A. Yartsev, V. Sundstrom and T. J. Savenije, *J. Am. Chem. Soc.*, 2015, **137**, 16043–16048.
26 G. Xing, N. Mathews, S. S. Lim, N. Yantara, X. Liu, D. Sabba, M. Gratzel, S. Mhaisalkar and T. C. Sum, *Nat. Mater.*, 2014, **13**, 476–480.
27 F. Deschler, M. Price, S. Pathak, L. E. Klintberg, D.-D. Jarausch, R. Higler, S. Huettner, T. Leijtens, S. D. Stranks, H. J. Snaith, M. Atatuere, R. T. Phillips and R. H. Friend, *J. Phys. Chem. Lett.*, 2014, **5**, 1421–1426.
28 Y. Yang, D. P. Ostrowski, R. M. France, K. Zhu, J. van de Lagemaat, J. M. Luther and M. C. Beard, *Nat. Photonics*, 2016, **10**, 53–59.
29 Y. Fang, Q. Dong, Y. Shao, Y. Yuan and J. Huang, *Nat. Photonics*, 2015, **9**, 679–686.
30 B. R. Sutherland, A. K. Johnston, A. H. Ip, J. Xu, V. Adinolfi, P. Kanjanaboos and E. H. Sargent, *ACS Photonics*, 2015, **2**, 1117–1123.
31 P. Piatkowski, B. Cohen, F. J. Ramos, M. Di Nunzio, M. K. Nazeeruddin, M. Graetzel, S. Ahmad and A. Douhal, *Phys. Chem. Chem. Phys.*, 2015, **17**, 14674–14684.
32 H.-Y. Hsu, C.-Y. Wang, A. Fathi, J.-W. Shiu, C.-C. Chung, P.-S. Shen, T.-F. Guo, P. Chen, Y.-P. Lee and E. W.-G. Diau, *Angew. Chem., Int. Ed.*, 2014, **53**, 9339–9342.
33 H. Kawai, G. Giorgi, A. Marini and K. Yamashita, *Nano Lett.*, 2015, **15**, 3103–3108.
34 M. Ziolek, I. Tacchini, M. T. Martinez, X. Yang, L. Sun and A. Douhal, *Phys. Chem. Chem. Phys.*, 2011, **13**, 4032–4044.
35 J. A. Arnaud, W. M. Hubbard, G. D. Mandevil, B. de la Claviere, E. A. Franke and J. M. Franke, *Appl. Opt.*, 1971, **10**, 2775–2776.
36 M. Saba, M. Cadelano, D. Marongiu, F. Chen, V. Sarritzu, N. Sestu, C. Figus, M. Aresti, R. Piras, A. G. Lehmann, C. Cannas, A. Musinu, F. Quochi, A. Mura and G. Bongiovanni, *Nat. Commun.*, 2014, **5**, 5049.
37 T. C. Sum, N. Mathews, G. Xing, S. S. Lim, W. K. Chong, D. Giovanni and H. A. Dewi, *Acc. Chem. Res.*, 2016, **49**, 294–302.
38 Y. Yang, M. Yang, Z. Li, R. Crisp, K. Zhu and M. C. Beard, *J. Phys. Chem. Lett.*, 2015, **6**, 4688–4692.
39 J. Even, L. Pedesseau and C. Katan, *J. Phys. Chem. C*, 2014, **118**, 11566–11572.
40 M. B. Price, J. Butkus, T. C. Jellicoe, A. Sadhanala, A. Briane, J. E. Halpert, K. Broch, J. M. Hodgkiss, R. H. Friend and F. Deschler, *Nat. Commun.*, 2015, **6**, 8420.
41 M. T. Weller, O. J. Weber, J. M. Frost and A. Walsh, *J. Phys. Chem. Lett.*, 2015, **6**, 3209–3212.

42 T. M. Koh, K. Fu, Y. Fang, S. Chen, T. C. Sum, N. Mathews, S. G. Mhaisalkar, P. P. Boix and T. Baikie, *J. Phys. Chem. C*, 2014, **118**, 16458–16462.
43 R. L. Milot, G. E. Eperon, H. J. Snaith, M. B. Johnston and L. M. Herz, *Adv. Funct. Mater.*, 2015, **25**, 6218–6227.
44 C. S. Ponseca, Jr., T. J. Savenije, M. Abdellah, K. Zheng, A. Yartsev, T. Pascher, T. Harlang, P. Chabera, T. Pullerits, A. Stepanov, J.-P. Wolf and V. Sundstrom, *J. Am. Chem. Soc.*, 2014, **136**, 5189–5192.
45 H. Wang, L. Whittaker-Brooks and G. R. Fleming, *J. Phys. Chem. C*, 2015, **119**, 19590–19595.
46 S. J. Yoon, K. G. Stamplecoskie and P. V. Kamat, *J. Phys. Chem. Lett.*, 2016, **7**, 1368–1373.
47 J. R. Klein, M. Scholz, K. Oum and T. Lenzer, *Phys. Chem. Chem. Phys.*, 2016, **18**, 10800–10808.
48 V. I. Klimov, *Annu. Rev. Phys. Chem.*, 2007, **58**, 635–673.
49 E. Istrate, S. Hoogland, V. Sukhovatkin, L. Levina, S. Myrskog, P. W. E. Smith and E. H. Sargent, *J. Phys. Chem. B*, 2008, **112**, 2757–2760.
50 C. La-o-vorakiat, T. Salim, J. Kadro, M.-T. Khuc, R. Haselsberger, L. Cheng, H. Xia, G. G. Gurzadyan, H. Su, Y. M. Lam, R. A. Marcus, M.-E. Michel-Beyerle and E. E. M. Chia, *Nat. Commun.*, 2015, **6**, 7903.
51 O. Flender, J. R. Klein, T. Lenzer and K. Oum, *Phys. Chem. Chem. Phys.*, 2015, **17**, 19238–19246.
52 C. Sheng, C. Zhang, Y. Zhai, K. Mielczarek, W. Wang, W. Ma, A. Zakhidov and Z. V. Vardeny, *Phys. Rev. Lett.*, 2015, **114**, 2189–2194.
53 M. J. Simpson, B. Doughty, B. Yang, K. Xiao and Y.-Z. Ma, *J. Phys. Chem. Lett.*, 2015, **6**, 3041–3047.
54 T. J. Savenije, C. S. Ponseca, Jr., L. Kunneman, M. Abdellah, K. Zheng, Y. Tian, Q. Zhu, S. E. Canton, I. G. Scheblykin, T. Pullerits, A. Yartsev and V. Sundstrom, *J. Phys. Chem. Lett.*, 2014, **5**, 2189–2194.
55 H. He, Q. Yu, H. Li, J. Li, J. Si, Y. Jin, N. Wang, J. Wang, J. He, X. Wang, Y. Zhang and Z. Ye, *Nat. Commun.*, 2016, **7**, 10896.
56 M. Joffre, D. Hulin, A. Migus and A. Antonetti, *J. Mod. Opt.*, 1988, **35**, 1951–1964.